EFFECTS OF BEYOND MEAN FIELD AND TENSOR FORCE ON GAMOW–TELLER AND β DECAY OF MAGIC NUCLEI*

Hiroyuki Sagawa

RIKEN, Nishina Center, Wako 351-0198, Japan
and
Center for Mathematics and Physics, University of Aizu, Fukushima, Japan

M.J. Yang, C.L. Bai

College of Physics, Sichuan University, Chengdu 610065, China

Received 9 December 2024, accepted 24 March 2025, published online 10 April 2025

We explore extensively new, and also long-standing, but still unsolved, nuclear structure problems by using beyond-mean-field model, Subtracted Second Random Phase Approximation (SSRPA). Firstly, the similarity between the subtraction method of SSRPA and Lee–Suzuki similarity transformation is pointed out to get the physical background of the SSRPA model. Secondly, we study the spin–isospin and electric excitations including the couplings to two-particle–two-hole states and the tensor correlations. Our results give a new insight into the quenching the of Gamow–Teller (GT) sum rule strengths without introducing any adjustable parameters in the self-consistent microscopic calculations. We further apply the SSRPA model to the β decay half-lives of four semi-magic and magic nuclei, ^{34}Si, ^{68,78}Ni, and ^{132}Sn. The inclusion of the two-particle–two-hole ($2p$–$2h$) configurations shifts low-lying GT states downwards. It leads to an increase of the β decay phase space, which ensures the half-lives of the four nuclei are finite and reduces the β decay half-lives dramatically. The effect of tensor interaction on the β decay half-life in the SSRPA model is also pointed out to change largely the half-lives by about one to two orders of magnitude with respect to the ones obtained without tensor force. The magnetic dipole transitions are also studied in the SSRPA model.

DOI:10.5506/APhysPolBSupp.18.2-A38

1. Introduction

The nuclear spin–isospin excitations are collective oscillations of the nucleus associated with the spin and isospin degree of freedom. They provide

* Presented at the 57$^{\text{th}}$ Zakopane Conference on Nuclear Physics, *Extremes of the Nuclear Landscape*, Zakopane, Poland, 25 August–1 September, 2024.

unique opportunity to study the spin–isospin correlations in nuclei [1, 2]. The GT excitation is the lowest order spin–isospin mode with the multiplicity and parity $J^\pi = 1^+$, which has been observed by the charge exchange reactions, such as (p, n), $(^3\mathrm{He}, t)$, and *vice versa*, and closely linked to the electron capture and β decay rates. The GT excitation has a strong impact on the r-process of nucleosynthesis together with the photonuclear cross sections [3]. In addition, the GT resonance is associated with double-β decay processes, especially for the two-neutrino double-β decay which take places through two GT-type transitions [4, 5]. The GT transition is related to the spin–isospin channel of the nucleon–nucleon interaction, and the precise description of the GT strength distribution is a significant mission for the microscopic nuclear theories.

The spin–isospin excitations have been discussed in terms of collectivity, the quenching of sum rule strength, the relation with elementally particle physics, and astrophysical relations. The main interests are listed as:

- Collectivity of spin and isospin excitations.
- Landau parameters of spin and spin–isospin channels g and g', which may imply the possible pion condensations at high nuclear density.
- SU(4) symmetry in light nuclei and the role of isoscalar ($T = 0$) pairing.
- Damping mechanism due to the configuration mixing.
- Effects of tensor correlations on magnetic dipole (M1) and GT excitations.
- Isobaric analogue state (IAS), charge symmetry breaking (CSB), and charge independence breaking (CIB) interactions.
- Super-allowed Fermi transitions and their implication on the Cabibbo–Kobayashi–Maskawa (CKM) unitarity matrix, which has been studied in the context of beyond Standard Model physics.
- Two-neutrino and neutrinoless double-beta decay.

Theoretically, the shell model and random phase approximation (RPA) are the models which are widely applied to study the spin–isospin excitations. The shell models are developed in various versions, such as the large-scale interacting shell model with realistic and phenomenological interactions, the *ab initio* no core shell model, the *ab initio* coupled cluster model, the Gamow shell model, the *ab initio* Green's function Monte Carlo (GFMC) shell model, and the Monte Carlo shell model (MCSM) with intrinsic deformed Slater determinants. The RPA models including self-consistent RPA based on the effective energy density functionals (EDFs), and conventional RPA models based on the realistic or Landau–Migdal interactions. There are also models beyond RPA:

— Particle-vibration coupling model (PVC, QPVC).
— Relativistic quasi-particle time blocking approximation (RQTBA).
— Coupled cluster model with singlet and doublet clusters (CCSD).
— Second RPA (SRPA), subtracted SRPA (SSRPA).
— Generator coordinate method (GCM).

In this manuscript I just report our researches of SSRPA due to the limitation of available pages.

2. Subtracted SRPA (SSRPA)

In this section, we briefly display the main formalism of SSRPA. More details can be found in several articles (see, for instance, Refs. [6, 7]). In the SRPA model, the excitation operator $Q^\dagger_\nu$ is given by

$$\begin{aligned} Q^\dagger_\nu &= \sum_{ph} \left(X^\nu_{ph} a^\dagger_p a_h - Y^\nu_{ph} a^\dagger_h a_p \right) \\ &\quad + \sum_{\substack{p_1<p_2 \\ h_1<h_2}} \left(X^\nu_{p_1p_2h_1h_2} a^\dagger_{p_1} a^\dagger_{p_2} a_{h_2} a_{h_1} - Y^\nu_{p_1p_2h_1h_2} a^\dagger_{h_1} a^\dagger_{h_2} a_{p_2} a_{p_1} \right) . \end{aligned} \quad (1)$$

The subscripts p, p_1, p_2 denote particle states, while h, h_1, h_2 are hole states. X and Y are forward and backward amplitudes. The SRPA equation has the same matrix form as that of the RPA equation

$$\begin{bmatrix} A & B \\ -B^* & -A^* \end{bmatrix} \begin{bmatrix} X^\nu \\ Y^\nu \end{bmatrix} = \hbar\omega_\nu \begin{bmatrix} X^\nu \\ Y^\nu \end{bmatrix} , \quad (2)$$

where A and B are matrices with double structure and X and Y are two column vectors

$$A = \begin{pmatrix} A_{11} & A_{12} \\ A_{21} & A_{22} \end{pmatrix} , \quad B = \begin{pmatrix} B_{11} & B_{12} \\ B_{21} & B_{22} \end{pmatrix} , \quad X = \begin{pmatrix} X^\nu_1 \\ X^\nu_2 \end{pmatrix} , \quad Y = \begin{pmatrix} Y^\nu_1 \\ Y^\nu_2 \end{pmatrix} . \quad (3)$$

The indices 1 and 2 are abbreviations for the $1p$–$1h$ and $2p$–$2h$ configurations, respectively. The matrix elements of Eq. (3) are expressed as

$$\begin{aligned} A_{11} &= A_{ph;p'h'} = \langle HF | \left[a^\dagger_h a_p, \left[H, a^\dagger_{p'} a_{h'} \right] \right] | HF \rangle \\ &= (E_p - E_h)\delta_{pp'}\delta_{hh'} + \bar{V}_{ph'hp'} , \end{aligned} \quad (4)$$

$$B_{11} = B_{ph;p'h'} = -\langle HF| \left[a_h^\dagger a_p, \left[H, a_{h'}^\dagger a_{p'}\right]\right] |HF\rangle = \bar{V}_{pp'hh'}\,, \tag{5}$$

$$A_{12} = A_{ph;p_1p_2h_1h_2} = \langle HF| \left[a_h^\dagger a_p, \left[H, a_{p_1}^\dagger a_{p_2}^\dagger a_{h_2} a_{h_1}\right]\right] |HF\rangle\,, \tag{6}$$

$$A_{22} = A_{p_1p_2h_1h_2;p_1'p_2'h_1'h_2'} = \langle HF| \left[a_{h_1}^\dagger a_{h_2}^\dagger a_{p_2} a_{p_1}, \left[H, a_{p_1'}^\dagger a_{p_2'}^\dagger a_{h_2'} a_{h_1'}\right]\right] |HF\rangle\,, \tag{7}$$

where E_p and E_h are the HF particle and hole energies, respectively, and $\bar{V}$ is the residual interaction. The quasi-boson approximation (QBA) is used in the derivation of matrix elements, and it turns out that B_{12}, B_{21}, and B_{22} have no contributions to the SRPA matrices.

It is well-known that the SRPA has a convergence problem; a larger model space makes a lower energy spectrum than the physical energy region. To cure this problem, the subtraction method was proposed. This procedure will start from the convolution of the $2p$–$2h$ model space into the $1p$–$1h$ model space. Then we get the energy-dependent matrices A and B for the $1p$–$1h$ model space as

$$\begin{aligned} A_{11'}(\omega) &= A_{11'} + \sum_2 A_{12}(\omega + i\eta - A_{22})^{-1} A_{21'} \\ &\quad + \sum_2 B_{12}(\omega + i\eta - A_{22})^{-1} B_{21'}\,, \\ B_{11'}(\omega) &= B_{11'} + \sum_2 A_{12}(\omega + i\eta - A_{22})^{-1} B_{21'} \\ &\quad + \sum_2 B_{12}(\omega + i\eta - A_{22})^{-1} A_{21'}\,. \end{aligned} \tag{8}$$

Two additional terms are ω-dependent and will induce non-convergence of SRPA because $A_{11'}(\omega)$ and $B_{11'}(\omega)$ for the $1p$–$1h$ model space depend on the size of the $2p$–$2h$ model space and, consequently, the SRPA solutions also depend on the model space. To cure this problem, the A and B matrices in the SRPA (2) are modified as

$$\begin{aligned} A^{\rm S}_{11'} &= A_{11'} + \sum_2 A_{12}(A_{22})^{-1} A_{21'} + \sum_2 B_{12}(A_{22})^{-1} B_{21'}\,, \\ B^{\rm S}_{11'} &= B_{11'} + \sum_2 A_{12}(A_{22})^{-1} B_{21'} + \sum_2 B_{12}(A_{22})^{-1} A_{21'}\,. \end{aligned} \tag{9}$$

Notice that the extra terms in Eq. (9) cancel exactly with the additional terms in Eq. (8) in the static limit $\omega \to 0$. This subtraction method is unavoidable since EDF was constructed originally to reproduce nuclear structure observables in the mean-field levels such as HF and RPA.

2.1. Lee–Suzuki similarity transformation and SSRPA

The coupled cluster model with singlet and doublet pairs (CCSD) is a similar approach to SRPA to include $2p$–$2h$ configurations on top of $1p$–$1h$ configurations. The essential difference is that the interaction is renormalized according to the size of the model space by using a similarity transformation (Lee–Suzuki) or the similarity renormalization group (SRG) technique [8]. According to the Lee–Suzuki method, we start from a many-body system which is described by the Schrödinger equation

$$H|\Psi\rangle = E|\Psi\rangle \tag{10}$$

with the *ab initio* Hamiltonian

$$H = H_0 + V\,, \tag{11}$$

where H_0 is the one-body Hamiltonian, V is the residual interaction, and $|\Psi\rangle$ is the exact wave function and E is the exact eigenvalue. In standard interacting shell models, the full model space is separated into two parts: active space denoted P space, and the inactive space called Q space. We define the projection operators P and Q, which project out each space, and satisfy

$$P + Q = 1\,, \qquad PQ = 0\,. \tag{12}$$

In the mean-field model, we define the P space as the $1p$–$1h$ model space and Q space as mp–mh states with $m = 2, 3, \ldots$ The operators P and Q satisfy the commutation relations with H_0

$$[P, H_0] = [Q, H_0] = 0\,, \tag{13}$$

and are called eigenprojectors. Consequently, we can obtain

$$PH_0Q = QH_0P = 0\,. \tag{14}$$

The objective of the Lee–Suzuki is to construct an effective Hamiltonian H_{eff} from the full Hamiltonian H, which acts only in the P space and satisfies the condition that any eigenvalue of H_{eff} should be one of the exact eigenvalues of the full Hamiltonian H. A general equation for determining H_{eff} can be derived by the use of the similarity transformation theory. We consider a similarity transformation of the Hamiltonian H

$$\mathcal{H} = X^{-1}HX\,, \tag{15}$$

where X is a transformation operator which is defined in the entire Hilbert space. The operator X is not unitary, but has its inverse X^{-1}. The transformed Hamiltonian $\mathcal{H}$ is decomposed into four terms

$$\mathcal{H} = (P+Q)\mathcal{H}(P+Q) = P\mathcal{H}P + Q\mathcal{H}P + P\mathcal{H}Q + Q\mathcal{H}Q\,. \tag{16}$$

To drive the effective Hamiltonian,

$$H_{\text{eff}} = P\mathcal{H}P = P\left(X^{-1}HX\right)P \tag{17}$$

from Eq. (16), we require a condition

$$Q\mathcal{H}P = Q\left(X^{-1}HX\right)P = 0\,. \tag{18}$$

Equation (18) provides the necessary and sufficient condition for the determination of H_{eff}, which has the eigenstate in P space corresponding to exactly one of the exact eigenstates of the full Hamiltonian H. We can prove this statement by the similarity transformation theory in the eigenvalue problem. If X is a solution of Eq. (18), H_{eff} in Eq. (17) satisfies

$$H_{\text{eff}}|\phi\rangle = \mathcal{H}|\phi\rangle \tag{19}$$

for any state ϕ in the P space so that H_{eff} is equivalent to $\mathcal{H}$ in the P space. Therefore, the eigenvalue of H_{eff} becomes also the eigenvalue of H. This means that the eigenvalue of H_{eff} agrees with one of the eigenvalues of the full Hamiltonian H because the similarity transformation does not change the eigenvalues.

The operator X is conveniently expressed as

$$X = \mathrm{e}^{\omega}\,, \tag{20}$$

where the operator ω has properties

$$\omega = Q\omega P \neq 0\,, \qquad P\omega P = Q\omega Q = P\omega Q = 0 \tag{21}$$

since ω is introduced to act as transformation from the P space to the Q space. From the properties of Eq. (21), Eq. (20) is simplified to

$$X = 1 + \omega\,, \tag{22}$$

since $\omega^2 = \omega^3 = \cdots = 0$.

The effective Hamiltonian is rewritten to be

$$H_{\text{eff}} = P\mathcal{H}P = PHP + PVQ\omega\,, \tag{23}$$

by using the properties of the operator ω. Then the effective interaction is given by

$$V_{\text{eff}} = H_{\text{eff}} - PH_0P = PVP + PVQ\omega\,. \tag{24}$$

The Hamiltonian H_{eff} has the eigenvalue E_i and the corresponding eigenstate $|\phi_i\rangle$ as

$$H_{\text{eff}}|\phi_i\rangle = (PH_0P + V_{\text{eff}})|\phi_i\rangle = E_i|\phi_i\rangle\,, \tag{25}$$

and the operator ω is expressed as [8]

$$\omega = \sum_{i}^{d} \omega(E_i)|\phi_i\rangle\langle\phi_i| \,, \quad \text{with} \quad \omega(E_i) = \frac{1}{E_i - QHQ}\, QVP \,, \tag{26}$$

where d is the dimension of the P space. Eventually, the effective interaction of the P space is expressed as

$$V_{\text{eff}} = PVP + \sum_{i}^{d} PVQ \frac{1}{E_i - QHQ}\, QVP\, |\phi_i\rangle\langle\phi_i| \,. \tag{27}$$

The eigenstate of full model space is also expressed as

$$|\Psi_i\rangle = \mathrm{e}^{\omega}|\phi_i\rangle = |\phi_i\rangle + \omega(E_i)|\phi_i\rangle \,. \tag{28}$$

Notice that the eigenenergy of the P space E_i is the same as that of full space eigenstate $|\Psi_i\rangle$.

The similarity transformation provides the renormalization term in V_{eff} in Eq. (27), which is exactly the same functional form as the subtraction term in SSRPA. Since EDF and the effective Lagrangian include the renormalization term from the beginning, it is physically justified to subtract the corresponding term if one expands the model space from the P space to the P+Q space. The adiabatic limit $\omega \to 0$ should be also reasonable since EDF is optimized for the data set of nuclear ground state and nuclear matter.

2.2. Convergence of SSRPA

For the present HF+SSRPA model, numerical details are found elsewhere [7, 9, 10]. The IS 0^+ strength distribution of ^{16}O calculated with SGII are shown in Fig. 1. All the discrete results are smoothed with the Lorentzian function having 1 MeV width. In the upper panel, the SSRPA$_D$ calculations are performed with the $2p$–$2h$ energy cutoff $E_{\text{cut}} = 60$, 70, and 80 MeV taking only the diagonal matrix elements of A_{22} in the subtraction procedure. One can find a good convergence of the strength distribution in the energy region lower than 20 MeV, and a reasonable convergence in the higher-energy region. The lower panel shows the strength distributions obtained by the SSRPA$_D$ and SSRPA$_F$ calculations with the energy cutoff of 60 MeV. All the matrix elements between $2p$–$2h$ configurations are included in SSRPA$_F$. We can see that the simplification in SSRPA$_D$ calculations causes only a small effect. However, we adopt full calculations SSRPA$_F$ for the latter M1, GT states, and also β decay study, so as to obtain more precise results.

We checked the isoscalar 0^+ and 2^+ energy moments m_1 and m_{-1} obtained by RPA and SSRPA calculations with the SGII interaction. As was already reported in Ref. [6], the m_1 moments are not conserved in the

SSRPA calculations compared to RPA, due to the subtraction procedure, while the m_{-1} moments are conserved by the SSRPA$_F$, being almost identical to the RPA ones. The conservation of m_{-1} moments was slightly broken in SSRPA$_D$ calculations by the diagonalization approximation.

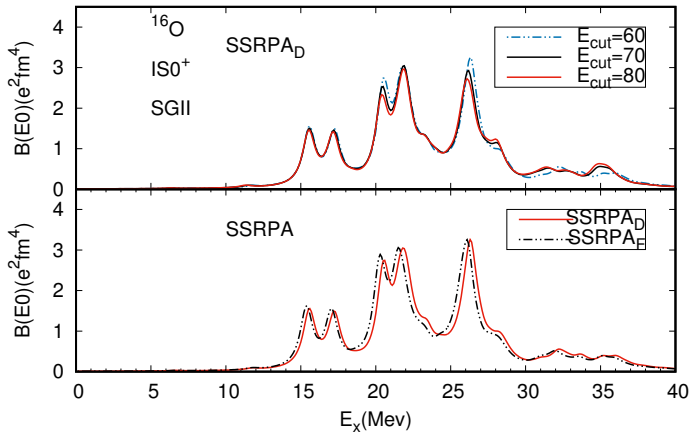

Fig. 1. (Color online) IS 0^+ strength distributions for ^{16}O calculated by SSRPA$_D$ calculations by SGII interaction with the $2p$–$2h$ energy cutoff $E_{\rm cut}$ = 60, 70, and 80 MeV (upper panel), and by SSRPA$_D$ and SSRPA$_F$ calculations at $E_{\rm cut}$ = 60 MeV (lower panel). See the text for more details.

3. Application of SSRPA for spin–isospin modes

We applied SSRPA for the spin–isospin excitations and β decay. In this contribution, we present results of magnetic dipole transitions (M1) and β decays of semi-magic nuclei.

3.1. Magnetic dipole transition in ^{48}Ca

We first investigate the role of tensor interactions on the HF p–h excitations energies and RPA correlation [9]. We tabulate the unperturbed p–h and RPA M1 excitation energies of SGII-T and SAMi-T without and with the tensor interactions for ^{48}Ca in Table 1. The tensor part of SAMi-T was determined guided by the *ab initio* relativistic Brueckner–Hartree–Fock (RBHF) studies on neutron–proton drops [11], and the beta decay half-lives in semi-magic nuclei by SSRPA calculations [9]. The dominant p–h configuration is $(1f_{7/2} \to 1f_{5/2})_\nu$ for ^{48}Ca so that the orbital operator has no contribution to the M1 strength. The M1 operator reads

$$\hat{O}(\mathrm{M1}) = \sum_i (g_s(i)\boldsymbol{s}_i + g_l(i)\boldsymbol{l}_i)\,, \tag{29}$$

where $g_s(i)$ ($g_l(i)$) is the spin (orbital) g factor given by $g_s(p) = 5.586$ ($g_l(p) = 1.0$) for protons and $g_s(n) = -3.826$ ($g_l(n) = 0.0$) for neutrons, respectively, in a unit of nuclear magneton μ_N. In the HF level, the triplet-odd term U acts uniquely on the energy splitting of neutron spin–orbit partners [12]. The large negative U value increases the spin–orbit splitting of similar particles so that the tensor interaction of SGII+T having a larger negative U gives much larger spin–orbit splitting compared with that of SAMi-T as is seen in Table 1. The strong triplet-odd term U affects also largely on the RPA correlations pushing upwards the excitation energies of M1 states in ^{48}Ca [9].

Table 1. The excitation energy of 1^+ state in ^{48}Ca. The energy is calculated with SGII+$(T, U) = (500, -280)$ and SAMi-T,$(T, U) = (415.5, -91.4)$ without and with tensor terms. ΔE^{T} is the difference of energies between with and without the tensor interaction, while ΔE(RPA-HF) (ΔE(SSRPA-HF) is the difference between RPA (SSRPA) and HF energies. The experimental excitation energy is 10.23 MeV. The unit is in MeV. See the text for details.

SGII	HF	RPA	ΔE(RPA-HF)	SSRPA	ΔE(SSRPA-HF)
w/o	6.44	8.90	2.46	7.34	0.90
with	9.25	11.35	2.10	9.05	−0.20
ΔE^{T}	2.81	2.45		1.71	
SAMi-T	HF	RPA	ΔE(RPA-HF)	SSRPA	ΔE(SSRPA-HF)
w/o	6.18	8.61	2.43	7.88	1.70
with	7.01	9.40	2.39	8.34	1.33
ΔE^{T}	0.83	0.46		−0.37	

Figure 2 shows the strength distributions and corresponding cumulative sums of the M1 resonance in ^{48}Ca calculated by RPA and SSRPA with SGII+T including tensor terms or not. The cumulative sums of B(M1) are counted up to $E_{\mathrm{max}} = 15$ MeV. The effects of the $2p$–$2h$ configuration mixings in SSRPA are clear in this figure. The RPA calculations either with or without tensor terms produce the main peak with a strength larger than $10\mu_N^2$, which is more than two times larger than the experiment data. In SSRPA calculations, the M1 strengths are reduced largely, and the strength of the main peak ($\simeq 4.09\ \mu_N^2$) becomes almost the same as the experimental one ($\simeq 4.0\ \mu_N^2$). Besides the main peak, some states with small strength are distributed around the main peak in SSRPA. The tensor terms shift the main peak energy upwards by about 1.7 MeV in SSRPA, which is still about 1 MeV lower than the experimental one. Figure 2 (d) indicates that the cumulative sum of B(M1) up to 15 MeV is reduced by more than 15% by the tensor correlations.

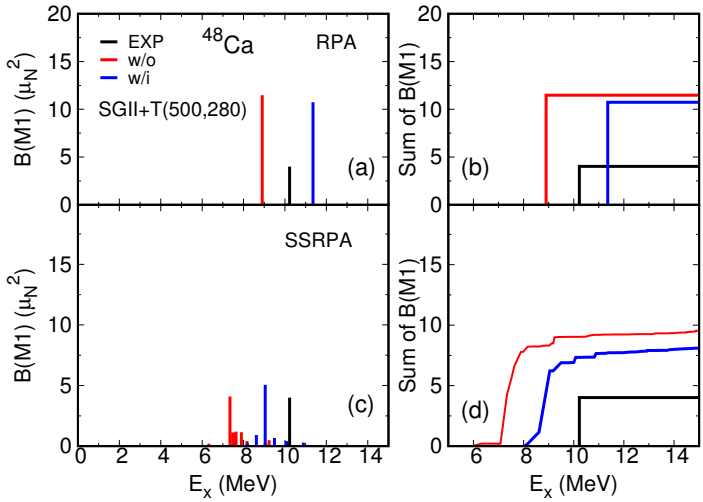

Fig. 2. (Color online) Strength distributions (left panels) and corresponding cumulative sums (right panels) of M1 excitations in ^{48}Ca calculated with the SGII, SGII+T(500, −280) EDFs by RPA (upper panels) and SSRPA (lower panels). The results obtained by SGII and SGII+T(500, −280) are shown by red/gray and blue/dark gray lines, respectively. The experimental data [13] are shown by the black lines. See the text for details.

Experimentally, the B(M1) strength of ^{48}Ca is dominantly measured at $Ex = 10.2$ MeV [13–17]. The measured total B(M1) strengths in several experiments are shown with the calculated results with different EDFs by RPA and SSRPA in Fig. 3. One can find that the calculated strengths by SSRPA are much smaller than those of RPA. It is seen that the tensor terms of SAMi-T give a small effect on the summed strength, while those of SGII+T(500, −280) and SGII+Te1(500, −350) reduce the summed strength by more than 10%, and provide tresults close to the (γ, n) experimental data.

3.2. β-decay lifetime

The GT-type β-decay half-life can be calculated using a formula [18]

$$T_{1/2} = \frac{D}{g_{\rm A}^2 \sum_n B^{\rm GT^-}_{1^+_n} f_0(Z, A, \omega_n)}\,, \tag{30}$$

where $D = 6163.4 \pm 3.8$ s, $g_{\rm A} \equiv G_{\rm A}/G_{\rm V} = 1.26$ is the ratio of the axial-vector to vector coupling constants, $B^{\rm GT^-}_{1^+_n}$ is the Gamow–Teller strength of $n^{\rm th}$ excited state with the energy ω_n referred to as the ground state of the

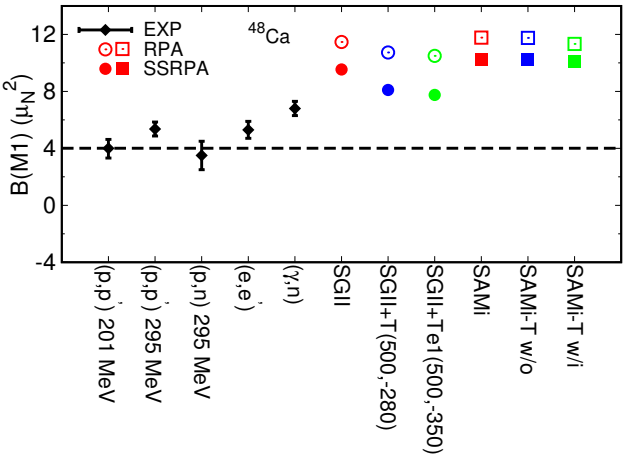

Fig. 3. (Color online) The cumulative sums of B(M1) strength up to $Ex = 15$ MeV in ^{48}Ca calculated by RPA (empty symbols) and SSRPA (filled symbols) with SGII, SGII+T($T = 500, U = -280$), SGII+Te1($T = 500, T = -350$), SAMi, SAMi-T EDFs, with or without tensor force. The results obtained by SGII, SGII+T, and SGII+Te1 are shown by red/gray, blue/dark gray, and green/light gray circles, respectively. The results obtained by SAMi, SAMi-T($T = 415.45, U = -95.53$) without or with tensor force are shown by red/gray, blue/dark gray, and green/light gray squares, respectively. The experimental data [13–17] are shown by the black squares with error bars.

mother nucleus. The Gamow–Teller operator is defined as operator

$$\hat{O}^{-}(\mathrm{GT}) = \sum_{i} t_{-}(i)\boldsymbol{\sigma}(i)\,. \tag{31}$$

The factor $f_0(Z, A, \omega_n)$ is the integrated phase factor at the energy ω_n. The value g_{A} is usually set to lower than 1.26 assuming a quenching factor which is closely related to the GT sum rule deficiency [19]. In this work, the value g_{A} is set to be $g_{\mathrm{A}} = 1.0$ [10]. This value is consistent with the quenching factor in our previous work on the study of GT transition strengths by the SSRPA model [7]. We study the effect of the $2p$–$2h$ correlations on the β-decay half-live of the four semi-magic and magic nuclei ^{132}Sn, ^{68}Ni, ^{34}Si, and ^{78}Ni. Figure 4 shows the β-decay half-lives calculated by the RPA and SSRPA models, in comparisons with experimental values. The RPA results largely overestimate the half-lives for almost all nuclei. For example, ^{132}Sn has an infinite lifetime in RPA calculations of all EDFs. On the other hand, the half-lives of all nuclei calculated with SSRPA become finite values, and agreement with the experimental values are much improved. In Fig. 4, the

SSRPA results of SLy5 and SkM* EDFs give better agreement of the half-lives than the other EFDs. Similar improvements in β-decay descriptions were obtained by the RPA+PVC calculations [20].

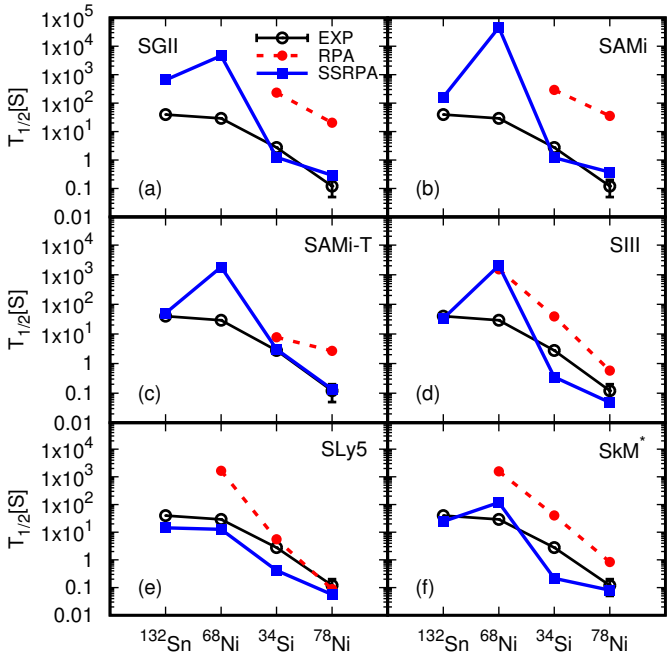

Fig. 4. (Color online) The β decay half-lives of ^{132}Sn, ^{68}Ni, ^{34}Si, and ^{78}Ni calculated by RPA and SSRPA models, respectively, in comparisons with experimental values [21]. The red/gray solid circles and the blue/dark gray solid squares represent results obtained by RPA and SSRPA respectively. The experimental data are shown by the black empty circles. The RPA results are infinite in some nuclei and not shown in the figure.

Figure 5 shows the β-decay half-lives calculated by RPA and SSRPA with SGII, SGII+T$(500, -280)$. The tensor terms reduce the half-lives in ^{34}Si and ^{78}Ni largely on the RPA level, but cannot give finite lifetimes for ^{68}Ni and ^{132}Sn. The effects of including $2p$–$2h$ configurations in SSRPA with SGII reduce the β-decay half-lives in ^{78}Ni and ^{34}Si by two orders of magnitude, and give finite half-lives for ^{132}Sn and ^{68}Ni. The effect of tensor force in SSRPA calculations is clearly observed in ^{68}Ni, where the tensor force reduces the half-live by two orders of magnitude, while the tensor force shows a minor effect on the half-life.

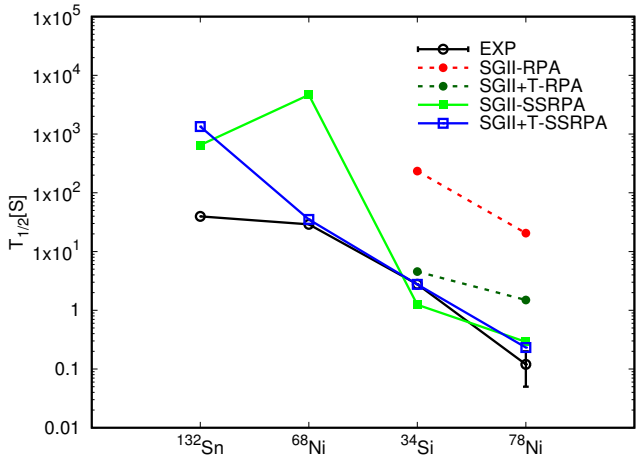

Fig. 5. (Color online) The β-decay half-lives of ^{132}Sn, ^{68}Ni, ^{34}Si, and ^{78}Ni calculated by RPA and SSRPA with SGII including or excluding tensor terms in comparison with the experimental values [21]. Six different EDFs are employed to study the model dependence of calculated results. The red/gray and dark green/dark gray filled circles represent results obtained by RPA with SGII and SGII+T, respectively, labeled "SGII-RPA" and "SGII+T-RPA". The green/light gray filled squares represent SSRPA results with SGII. The blue/dark gray open squares represent SSRPA results with SGII+T. The experimental data are shown by the black open circles.

4. Summary

We first discuss the similarity between the subtraction procedure SSRPA and the similarity transformation by the Lee–Suzuki method for beyond mean field calculations. Namely, the subtracted matrix elements of SSRPA from the $1p$–$1h$ model space correspond to the renormalization terms from the Q space to the effective interaction of the P space. This similarity may justify the subtraction procedure of SSRPA. The convergence of the SSRPA model is checked for the calculations of the natural parity excitations 0^+ and 2^+ states in ^{16}O and ^{40}Ca, changing the model space. We found good convergence for the excited spectra up to $Ex = 30$ MeV and also the inverse energy weighted sum rule value.

We applied the SSRPA model to describe the magnetic dipole states, Gamow–Teller states, and β decays. It is pointed out the quenching of M1 and GT states are largely explained by the couplings to $2p$–$2h$ states. On top of that, the tensor interaction contributes 5–10% effect to induce further the quenching effect. The β-decay life-times of semi-magic and magic nuclei

were also studied in the SSRPA model and a large improvement of the lifetime predictions is found in these nuclei compared with the standard RPA calculations.

REFERENCES

[1] M.N. Harakeh, A. van der Woude, «Giant Resonances: Fundamental High-Frequency Modes of Nuclear Excitation», *Oxford University Press*, Oxford 2001.

[2] M. Ichimura, H. Sakai, T. Wakasa, *Prog. Part. Nucl. Phys.* **56**, 446 (2006).

[3] T. Kajino *et al.*, *Prog. Part. Nucl. Phys.* **107**, 109 (2019).

[4] F.T. Avignone, S.R. Elliott, J. Engel, *Rev. Mod. Phys.* **80**, 481 (2008).

[5] J. Engel, J. Menéndez, *Rep. Prog. Phys.* **80**, 046301 (2017).

[6] D. Gambacurta, M. Grasso, J. Engel, *Phys. Rev. C* **92**, 034303 (2015).

[7] M.J. Yang, H. Sagawa, C.L. Bai, H.Q. Zhang, *Phys. Rev. C* **106**, 014319 (2022).

[8] K. Suzuki, S.Y. Lee, *Prog. Theor. Phys.* **64**, 2091 (1980).

[9] M.J. Yang, H. Sagawa, C.L. Bai, H.Q. Zhang, *Phys. Rev. C* **107**, 014325 (2023).

[10] M.J. Yang, C.L. Bai, H. Sagawa, H.Q. Zhang, *Phys. Rev. C* **109**, 054319 (2024).

[11] S. Shen, G. Colò, X. Roca-Maza, *Phys. Rev. C* **99**, 034322 (2019).

[12] G. Colò, H. Sagawa, S. Fracasso, P.F. Bortignon, *Phys. Lett. B* **646**, 227 (2007); H. Sagawa, G. Colò, *Prog. Part. Nucl. Phys.* **76**, 76 (2014).

[13] J. Birkhan *et al.*, *Phys. Rev. C* **93**, 041302(R) (2016).

[14] W. Steffen *et al.*, *Phys. Lett. B* **95**, 23 (1980).

[15] W. Steffen *et al.*, *Nucl. Phys. A* **404**, 413 (1983).

[16] J.R. Tompkins *et al.*, *Phys. Rev. C* **84**, 044331 (2011).

[17] M. Mathy *et al.*, *Phys. Rev. C* **95**, 054316 (2017).

[18] J. Engel *et al.*, *Phys. Rev. C* **60**, 014302 (1999).

[19] E. Caurier *et al.*, *Rev. Mod. Phys.* **77**, 427 (2005).

[20] Y.F. Niu, Z.M. Niu, G. Colò, E. Vigezzi, *Phys. Rev. Lett.* **114**, 142501 (2015).

[21] `http://www.nndc.bnl.gov`